Available online at www.sciencedirect.com
ScienceDirect
Ceramics International 37 (2011) 2247–2253
CERAMICS INTERNATIONAL
www.elsevier.com/locate/ceramint

Dependence of photocatalytic activity on structural and optical properties of nanocrystalline ZnO powders

Sumetha Suwanboon [a,*], Pongsaton Amornpitoksuk [b], Nantakan Muensit [c]

[a] Department of Materials Science and Technology, Faculty of Science, Prince of Songkla University, Hat Yai, Songkhla 90112, Thailand
[b] Department of Chemistry and Center for Innovation in Chemistry, Faculty of Science, Prince of Songkla University, Hat Yai, Songkhla 90112, Thailand
[c] Department of Physics, Faculty of Science, Prince of Songkla University, Hat Yai, Songkhla 90112, Thailand

Received 19 January 2011; received in revised form 4 March 2011; accepted 7 March 2011
Available online 16 March 2011

Abstract

Nanocrystalline ZnO powders were prepared from cetyltrimethylammonium bromide (CTAB)-modified NaOH, NH_4OH and $(CH_2)_6N_4$ solutions. The calcined ZnO powders exhibited a hexagonal structure without any secondary phase. Different shapes of ZnO powders were formed depending on CTAB concentration and type of precipitating agent. As $(CH_2)_6N_4$ solution was used, rod-like ZnO structure was changed to a spherical shape when CTAB concentration was increased. The widest E_g value of approximately 3.23 eV was obtained from the sample containing the lowest defect concentration. The decolorization efficiency was higher than 90% after irradiating for 90 min and the sample with higher E_g value showed higher decolorization efficiency.

Keywords: A. Powders: chemical preparation; C. Chemical properties; C. Optical properties; D. ZnO

1. Introduction

ZnO is normally an *n*-type II–VI semiconductor with a wide band gap of about 3.2 eV and a large exciton binding energy of 60 meV [1]. Consequently, ZnO is one of the candidates for optoelectronic devices [2,3], solar cell [4] and photocatalytic applications [5]. In recent years, it has been found that ZnO can be synthesized by various routes such as vapor phase [6], sonochemical [7], sol–gel [4] and precipitation [1] methods. Among these methods, precipitation has many advantages over the other methods, for example, it is unsophisticated and a low cost method. Moreover, the morphology of ZnO powders can be controlled easily by using an appropriate surfactant or capping agent such as polyvinylpyrolidone (PVP) [8], polyethylene glycol (PEG) [9], monoethanolamine (MEA), diethanolamine (DEA) or triethanolamine (TEA) [10], polyethylene oxide-block-polypropylene oxide (PEO-*b*-PPO) copolymer [1] and cetyltrimethylammonium bromide (CTAB) [11]. Furthermore, this method can be used for mass production. It is evident that the desired chemical and physical properties particularly the optical properties and photocatalytic activity strongly related to particle sizes and shapes of ZnO powders. Over the past years, many researchers have reported that ZnO powders have a more powerful photocatalytic reaction than TiO_2 because ZnO powders can absorb larger fractions of the solar spectrum over TiO_2 powders [12]. For this reason, many researchers have focused on synthesis of different morphologies of ZnO powders due to the fact that they displayed the unique properties.

In this study, we report the influence of CTAB concentration on formation of different ZnO morphologies via a precipitation method using sodium hydroxide (NaOH), ammonium hydroxide (NH_4OH) and hexamethylenetetramine ($(CH_2)_6N_4$, HMTA) as a precipitating agent. CTAB was studied because it can dissolve easily in water and because of the lack of documents the effect of CTAB-modified HMTA solution was not reported. We also compared the effect of CTAB-modified different bases on morphology formation. Furthermore, we also report the effects of particle sizes and shapes on optical properties and photocatalytic activity.

* Corresponding author. Tel.: +66 74 28 82 50; fax: +66 74 28 83 95.
E-mail address: ssuwanboon@yahoo.com (S. Suwanboon).

0272-8842/$36.00
doi:10.1016/j.ceramint.2011.03.016

2. Materials and methods

2.1. Materials

All chemicals were of analytical grade and they were used without further purification. Zinc nitrate hexahydrate ($Zn(NO_3)_2{\bullet}6H_2O$, Fluka) was used as a zinc source. HMTA ($C_6H_{12}N_4$, Fluka), NH_4OH (Carlo Erba) and NaOH (Carlo Erba) solutions were used as a precipitating agent and CTAB ($C_{19}H_{42}BrN$, Fluka) was used as a capping agent.

2.2. Experimental

To study the effect of each precipitating agent and CTAB concentration, 0.16 mol (6.4 g) NaOH, 0.16 mol (22.43 g) HMTA and 0.04 mol (1.58 ml) NH_4OH were first dissolved in 100 ml of distilled water in a conical flask separately. 0.01 and 0.02 mol (3.64 and 7.28 g) CTAB were then added into each precipitating agent solution and all conditions are presented in Table 1. After that, CTAB-modified precipitating agent solutions were magnetically stirred for 1 h until the homogenous solutions were obtained. 0.02 mol (5.95 g) $Zn(NO_3)_2{\bullet}6H_2O$ that was dissolved in 100 ml of distilled water, was finally added dropwise into each CTAB-modified precipitating agent solution. White precipitates were formed in the solutions and were heated at 70 °C under a magnetically stirring for 1 h. The precipitates were filtered, rinsed with distilled water and absolute ethanol, dried at room temperature and finally calcined at 600 °C in air for 1 h.

2.3. Characterizations

The ZnO formation was identified by an X-ray diffraction (XRD, X'Pert MPD, PHILIP) using Cu-K_α radiation ($\lambda = 1.5406$ Å). The morphology of ZnO powders was determined by a scanning electron microscope (SEM, JSM-5800LV, JEOL) with an acceleration voltage of 20 kV. The optical absorbance was measured by a UV-Vis spectrophotometer (UV-Vis 2450, Shimadzu) and the room temperature photoluminescence (PL) spectra were recorded by a luminescence spectrometer (LS/55, PerkinElmer).

Table 1
The experimental conditions and the crystallite size of all ZnO samples.

Precipitating agent	Sample code	CTAB (mole)	Crystallite size
NaOH (0.16 mole)	S1	0	46.4 ± 13.3
	S2	0.01	43.5 ± 6.6
	S3	0.02	41.3 ± 7.6
HMTA (0.16 mole)	S4	0	43.8 ± 3.5
	S5	0.01	42.6 ± 5.0
	S6	0.02	41.5 ± 6.2
NH_4OH (0.04 mole)	S7	0	42.2 ± 6.4
	S8	0.01	41.5 ± 6.2
	S9	0.02	39.9 ± 5.6

2.4. Photocatalytic test

The photocatalytic tests on the selected samples for decomposition of methylene blue (MB) solution were performed at ambient temperature. A Pyrex beaker (250 ml) was used as the photoreactor vessels. 150 mg of selected ZnO samples were added in 150 ml of 1×10^{-5} M aqueous methylene blue solution. The solutions were magnetically stirred in the dark for 30 min to ensure the establishment of adsorption/desorption equilibrium of methylene blue on the sample surfaces. The solutions were then exposed to a UV light. At given irradiation time intervals (30, 60, 90, 120 and 180 min), 3 ml of each aqueous solution was collected and centrifuged to remove the ZnO powders and was then analyzed on a Lambda 25 UV-Vis spectrometer. The concentration of aqueous methylene blue solution was determined by monitoring the change in the absorbance centered at 665 nm.

3. Results and discussion

3.1. Effect of synthetic conditions on structural properties

Fig. 1 shows XRD patterns of all calcined samples precipitated from different precipitating agents when CTAB was used as a capping agent. All the diffraction peaks can be indexed only as a diffraction pattern of hexagonal or wurtzite structure in good agreement with the JCPDS 36-1451 (space group $P6_3mc$ and lattice parameters: $a = b = 0.3249(8)$ and $c = 0.5206(6)$ nm), suggesting that the calcined samples are a pure ZnO phase without any secondary phase.

To study the effects of CTAB concentration on the morphology of ZnO, the crystallite size of all calcined ZnO powders was calculated from the XRD results by the Scherrer's formula [13]:

$$D = \frac{k\lambda}{\beta \cos\theta} \quad (1)$$

where D is the crystallite size, k is a shape factor constant ($k = 0.9$), λ is the wavelength of incident X-ray ($\lambda = 0.15406$ nm), θ is the Bragg angle of the diffraction line and β is the full width at half maximum (FWHM) in radian.

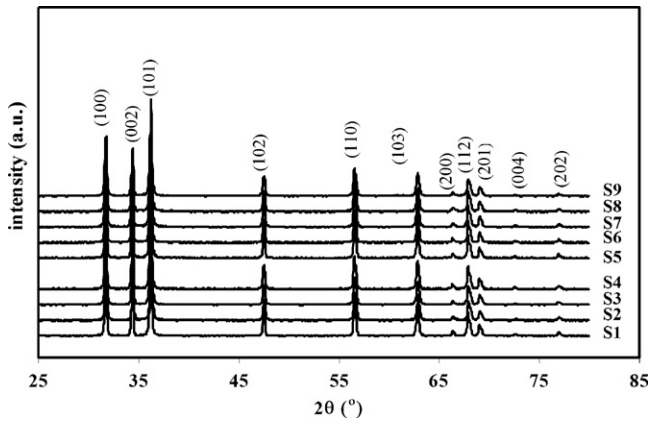

Fig. 1. XRD patterns of all ZnO samples.

It was observed that the crystallite size decreased as CTAB concentration was increased. As we know, CTAB is a cationic surfactant that can ionize completely in water to form a cationic head groups ($N(CH_3)_3^+$) and a long hydrophobic tail. The presence of 0.01 mol (0.025 M) and 0.02 mol (0.05 M) CTAB in the solutions is higher than its critical micelle concentration (0.94 mM), indicating that CTAB acts as a capping agent instead of forming the micelles [14]. For instance, the cationic head groups can be adsorbed on the surface of ZnO by electrostatic interaction and the strong interaction can either suppress the dissolution of ZnO particles or can inhibit the adsorption of dissolved Zn species presented in a bulk solution onto the ZnO surface. Therefore, the ZnO cannot grow any longer and smaller crystallite size was obtained when higher CTAB concentration was used.

The calcined ZnO powders with different shapes and sizes are presented in Fig. 2. The rod-like structure was shaped when NaOH and NH_4OH solutions were used as a precipitating agent. Nevertheless, the particle shape did not alter when CTAB was added into the NaOH and NH_4OH solutions. However, a rod diameter was diminished as a function of CTAB concentration. In contrast, the morphology strongly depended upon CTAB concentration when HMTA solution was used. The rod-like structure was altered to spherical shape when CTAB concentration was increased. To further understand why the different morphologies can form, the growth mechanisms were purposed for each system.

As NaOH solution was used, number of Zn species can form as reported in [15].

$$Zn^{2+} + OH^- \leftrightarrow Zn(OH)^+$$

$$Zn(OH)^+ + OH^- \leftrightarrow Zn(OH)_2$$

$$Zn(OH)_2 \leftrightarrow Zn^{2+} + 2OH^-$$

$$Zn(OH)_2 + OH^- \leftrightarrow Zn(OH)_3{}^-$$

$$Zn(OH)_2 + 2OH^- \leftrightarrow Zn(OH)_4{}^{2-}$$

$$Zn(OH)_4{}^{2-} \leftrightarrow ZnO + H_2O + 2OH^-$$

Under the strong alkaline NaOH solution, $Zn(OH)_4{}^{2-}$ species acted as a growth unit of ZnO. As a matter of fact, ZnO is a polar crystal, the O^{2-} and Zn^{2+} ions form a tetrahedral unit. Zn and oxygen atoms are arranged alternatively along the *c*-axis and some surfaces are either terminated with Zn^{2+} cations, exhibiting a positive polar plane Zn-(0 0 0 1) or terminated with O^{2-} anions, exhibiting a negative polar plane O-$(0\,0\,0\,\bar{1})$. In this study, a pH value of final solution (pH > 13.0) is higher than the point of zero charge (PZC) of ZnO (~9.5), so the surface of ZnO nuclei is surrounded by negatively charged species [16]

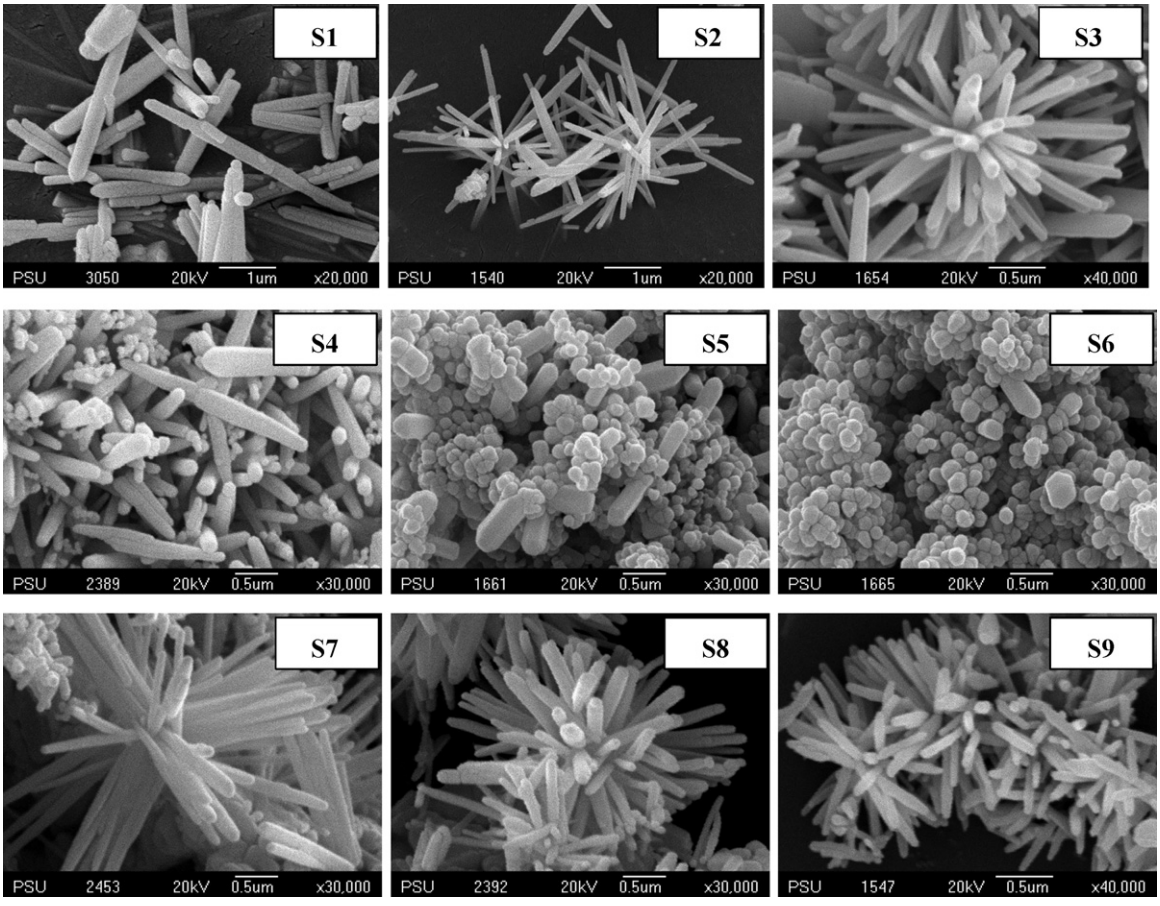

Fig. 2. SEM images of all ZnO samples.

and rod-like structure can grow along the *c*-axis owing to the more rapid growth rate that was found to be $v_{(0001)} > v_{(\bar{1}01\bar{1})} > v_{(\bar{1}010)} > v_{(\bar{1}011)} > v_{(000\bar{1})}$. Via the addition of CTAB in the solutions, the cationic head groups ($N(CH_3)_3^+$) could strongly adsorb on the ZnO facets by electrostatic interaction, giving rise to a further growth along the *c*-axis [17].

In the case of HMTA solution was used, a pH value of final solution is 8.8. Under this condition, rod-like ZnO structure was changed evidently to a spherical shape when the solution was modified by CTAB. From speciation diagram in [18], Zn^{2+} ions can interact with NH_3 and form a $[Zn(NH_3)_4]^{2+}$ complex at a pH value of 8.8. After that ZnO nuclei can form via dehydration reaction and the ZnO can grow preferentially along the *c*-axis or $\langle 0\,0\,0\,1\rangle$ direction because of its rapid growth rate as mentioned previously.

$$(CH_2)_6N_4 + 6H_2O \rightarrow 4NH_3 + 6HCHO$$

$$NH_3 + H_2O \leftrightarrow NH_4^+ + OH^-$$

$$Zn^{2+} + 4NH_3 \leftrightarrow [Zn(NH_3)_4]^{2+}$$

$$[Zn(NH_3)_4]^{2+} + 2OH^- \rightarrow ZnO + 4NH_3 + H_2O$$

Under these experiments, a pH value of final solution (8.8) is lower than the PZC of ZnO, so the surface of ZnO nuclei is surrounded by positively charged species. When the CTAB was added into the solution, both CTAB and ZnO crystal surface were positively charged at this pH. Therefore, the electrostatic interaction did not occur [19] but CTAB could promote the growth along the other planes, thus spherical shape can form under this condition.

As NH_4OH solution was used, a rod-like shape occurred in all experiments. A pH value of solutions (10.8) is a bit higher than the PZC of ZnO, thus the surface of ZnO is surrounded by the negatively charged species and therefore the electrostatic interaction can affect the rod-like formation as in the case of NaOH solution. The chemical reactions were followed and proposed based on the speciation diagram in [18].

$$NH_3 + H_2O \leftrightarrow NH_4^+ + OH^-$$

$$Zn^{2+} + 2OH^- \leftrightarrow Zn(OH)_2$$

$$Zn(OH)_2 + OH^- \leftrightarrow Zn(OH)_3^-$$

$$Zn(OH)_2 \leftrightarrow ZnO + H_2O$$

3.2. Band gap evaluation

In this part, the dependence of optical band gap on particle shape and size was studied. S1, S2 and S3 are representative samples to investigate the effect of crystallite size whereas S3 and S6 are representative samples to study the effects of particle shape.

In this study, the E_g value can be estimated from a linear portion of the $(\alpha E)^2$ versus E curves (Fig. 3(a)) plotted from the following equation [20]:

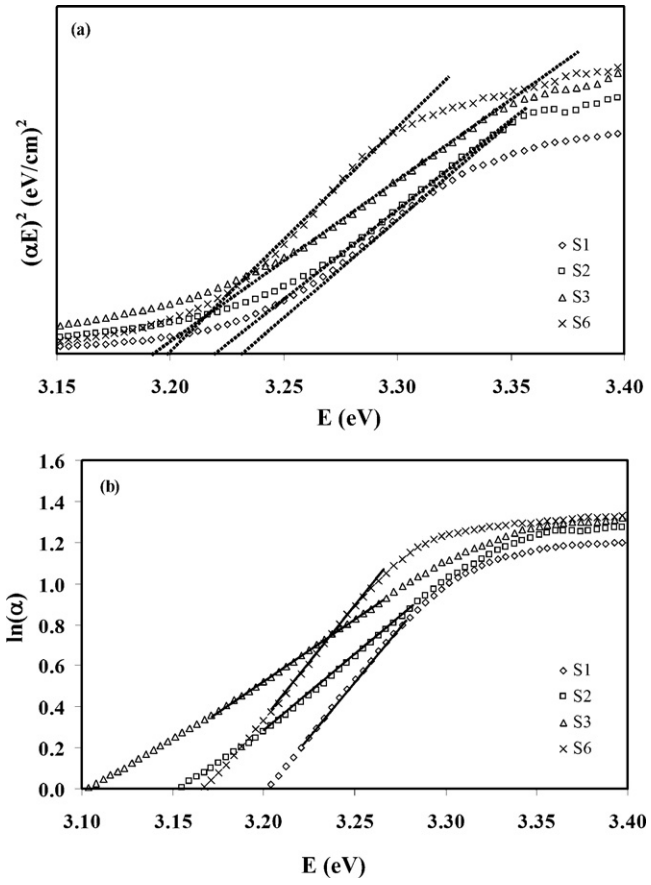

Fig. 3. (a) The evolution of band gap from the plots of $(\alpha E)^2$ vs. E and (b) the evolution of defect concentration from the plots of $\ln(\alpha)$ vs. E for ZnO samples with different sizes (S1–S3) and different shapes (S3 and S6).

$$(\alpha E)^2 = E_D(E - E_g) \tag{2}$$

where E is the photon energy, E_g is the optical band gap, E_D is a constant and α is an absorption coefficient that could be approximated by:

$$\alpha = \frac{A}{d} \tag{3}$$

where A is the measured absorbance and d is the thickness of the cell (0.4 cm) and E can be estimated by:

$$E = \frac{1240}{\lambda} \tag{4}$$

where λ is the measured wavelength (nm).

To investigate the effect of crystallite size, S1, S2 and S3 (rod-like structure) were selected so as to omit the shape effect. The estimated E_g value of these samples is presented in Table 2. It is evident that the E_g value decreased when the crystallite size decreased. It has been recognized that the E_g value occurred from an electronic transition between the filled valence bands to the empty conduction bands and ZnO single crystal normally shows the E_g value of about 3.37 eV. Obviously, the E_g value of all samples is smaller than that of the E_g value of a single crystal. This is due to the imperfections or defect formations

Table 2
The effect of particle size and shape on band gap energy and defect concentration.

Sample code	Crystallite size (nm)	E_g (eV)	E_0 (eV)
S1	46.4 ± 13.3	3.23	0.09
S2	43.5 ± 6.6	3.21	0.15
S3	41.3 ± 7.6	3.18	0.18
S6	41.5 ± 6.2	3.20	0.10

within a forbidden band of ZnO powders. So, the E_g value obtained from the electronic transition between the filled valence states to the energy level of the generated defects instead of the transition between the valence band to the conduction band as usual. To verify the defect, the room temperature PL spectra were measured in a range of 450–800 nm as presented in Fig. 4(a). A broad visible emission occurred by the envelop spectra of multiple emission bands originating from many defects such as zinc vacancy (V_{Zn}), zinc interstitial (Zn_i), oxygen vacancy ($V_{\dot{O}}$), oxygen interstitial (O_i), antisite oxygen (O_{Zn}), etc. [1]. Based on the spectra obtained, higher emission intensity obtained from a smaller size or higher surface area to volume ratio. In fact, ZnO has many defects on its surface which can adsorb O^{2-} and O^- ions to form oxygen vacancies. Therefore, it could be presumed, that the sample with a higher intensity has more defect concentration. In this study, S3 performed the highest emission intensity; it suggests that this sample has the highest defect concentration, so it is reasonable to conclude that this sample shows the smallest E_g value.

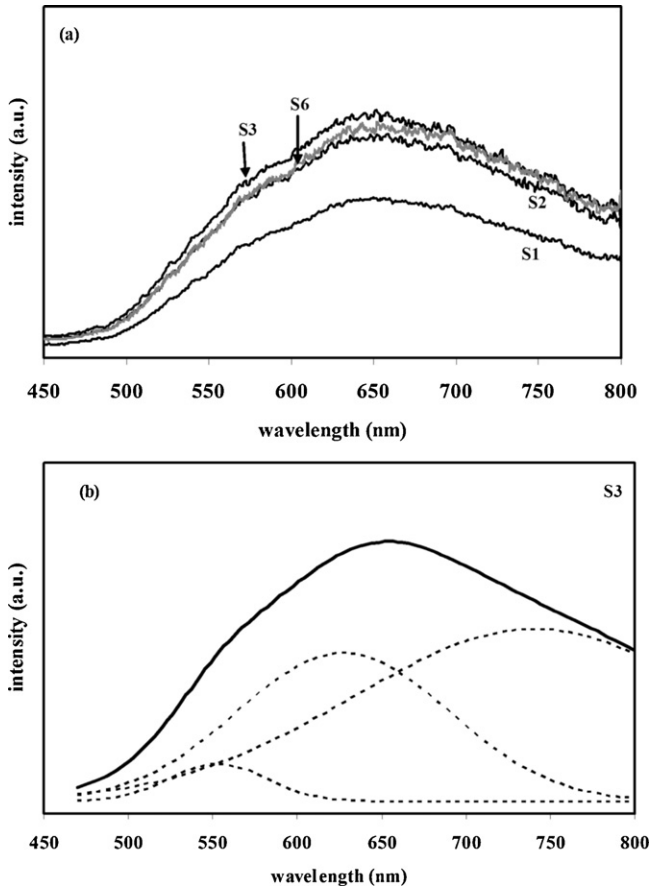

Fig. 4. (a) Room temperature PL spectra of ZnO samples with different sizes (S1–S3) and different shapes (S3 and S6) and (b) the fitting analysis using a Gaussian function of S3.

To study the influence of particle shape on E_g value, the S3 (rod-like) and S6 (spherical shape) were selected. The E_g value obtained from S6 (spherical shape) is higher than the E_g value obtained from S3 (rod shape). The room temperature PL spectra of S3 and S6 show slightly different emission intensity in the visible region as shown in Fig. 4(a). Therefore, the defect concentration (E_0) obtained from the reciprocal value of the slopes from the linear part of the curves of $\ln(\alpha)$ versus E was determined and the results are given in Table 2. From the results obtained, we can confirm that the E_g value depended upon the defect concentration. So, it could be pointed out that the sample with higher defect concentration gave a smaller E_g value.

Regarding S3, the broad band in the visible region (450–800 nm) was fitted with a Gaussian function as presented in Fig. 4(b). By the fitting result, a green band centered at about 540 nm is attributed to oxygen vacancies as well as yellow band (640 nm) and an infrared band (740 nm) are due to interstitial ions or extrinsic defects [21,22].

3.3. Photocatalytic activity

The temporal change in MB concentration for ZnO powders with different sizes and shapes are depicted in Fig. 5. It is clearly observed that the maximum absorbance of 665 nm decreased as a function of UV irradiation time. This is due to the breaking of the conjugated π-system in the MB chain [23], consequently very pale white solutions were obtained, indicating that the auxochromic groups were degraded. Fig. 6 shows the decolorization efficiency (%) of ZnO powders calculated by the following equation:

$$y\ (\%) = \frac{C_0 - C}{C_0} \times 100 \quad (6)$$

where y is the decolorization efficiency, C_0 is the initial MB concentration and C is the MB concentration after irradiation at a given time.

As can be seen, the decolorization efficiency of all samples increased when the irradiation time was increased and the decolorization efficiency was higher than 90% after irradiating for 90 min. After the suspensions were irradiated by the UV light with energy higher than the band gap, the electrons (e^-) in the valence band can be excited to the empty conduction band and the holes (h^+) occurred suddenly in the valence band. When the photoelectrons were trapped by oxygen that acted as an electronic acceptor and a superoxide radical anion ($^{\bullet}O_2^-$) were generated subsequently whereas the holes were trapped by MB and these holes acted as an electronic donor to oxidize the MB [24].

Considering the decolorization efficiency of S1, S2 and S3 after being irradiated for 90 min, it is evident that the sample with a rod-like shape and larger E_g value showed a great powerful oxidation of MB. This is because S1 has the largest E_g

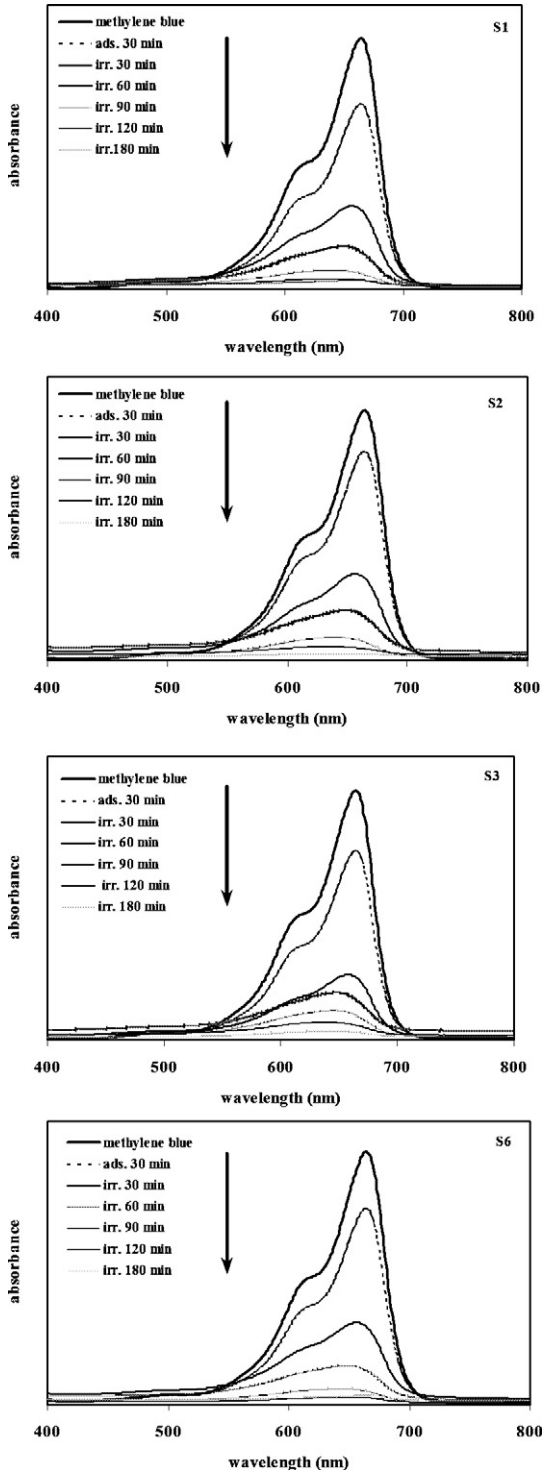

Fig. 5. Temporal change in the concentration of MB monitored from ZnO samples with different sizes (S1–S3) and different shapes (S3 and S6).

value, the photoinduced electrons can stabilize for a long time in the conduction band before coming back to the valence band or we can conclude that the sample with wider E_g value has an appropriate energy potentials of charge carriers that can conduct the redox potential on the sample surface via the separately photogenerated electrons and holes [25]. For this reason, the decolorization efficiency of S1 is higher than those of S2 and S3.

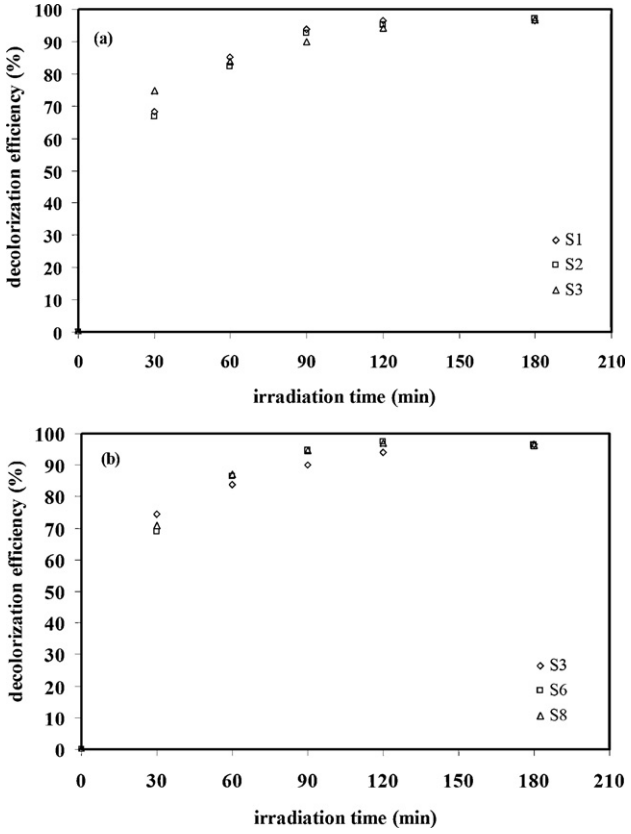

Fig. 6. The efficiency comparison of photocatalytic activity of ZnO samples with different sizes (S1–S3) and different shapes (S3 and S6).

S3 and S6 are representative samples to investigate the effects of particle shape. It was observed that the decolorization efficiency of S6 (spherical shape) after being irradiated for 90 min is stronger than that of S3 (rod-like shape). This is because S6 has a larger E_g value. Thus the decolorization efficiency is higher as mentioned above.

4. Conclusions

The different morphologies of ZnO powders were synthesized via precipitation method by using NaOH, HMTA and NH_4OH as the precipitating agent. In this study, CTAB concentration was higher than its critical micelle concentration, so it acted as a capping agent instead of a micelle formation. The size of ZnO powders decreased as CTAB concentration was increased because CTAB can encapsulate the ZnO powder powerfully. CTAB concentration strongly affected the shape formation when HMTA solution was used. It is evident that the rod-like was altered to spherical shape when CTAB concentration was increased. A larger E_g value was obtained from the sample containing a lower defect concentration. The photocatalytic degradation test suggested that ZnO powders showed a great powerful activity in dye degradation of over 90% after irradiating with the UV light for 90 min. The decolorization efficiency depended upon the E_g values of the samples. The higher efficiency obtained from the sample with larger E_g value

because of the retardation of the electron–hole recombination process.

Acknowledgements

This research is supported by Thailand Research Fund (TRF) under the contract number MRG5280125 and DIG54D0011. The authors would like to be thankful the Center for Innovation in Chemistry (PERCH-CIC), Commission on Higher Education, Ministry of Education and the authors would like to acknowledge Michael Benjamin Lane for proof reading our manuscript.

References

[1] N. Samaele, P. Amornpitoksuk, S. Suwanboon, Effect of pH on the morphology and optical properties of modified ZnO particles by SDS via a precipitation method, Mater. Lett. 64 (2010) 500–502.
[2] A.B. Djurisic, A.M.C. Ng, X.Y. Chen, ZnO nanostructures for optoelectronics: material properties and device applications, Quantum Electron. 34 (2010) 191–259.
[3] A. Chiappini, C. Armellini, A. Chiasera, M. Ferrari, R. Guider, Y. Yestin, L. Minati, E. Moser, G. Nunzi Conti, S. Pelli, R. Retoux, G.C. Righini, G. Speranza, Preparation and characterization of ZnO particles embedded in organic–inorganic planar waveguide by sol–gel route, J. Non-Cryst. Solids 355 (2009) 1132–1135.
[4] S. Rani, P. Suri, P.K. Shishodia, R.M. Mehra, Synthesis of nanocrystalline ZnO powder via sol–gel route for dye-sensitized solar cells, Sol. Energy Mater. Sol. Cells 92 (2008) 1639–1645.
[5] J.H. Sun, S.Y. Dong, Y.K. Wang, S.P. Sun, Preparation and photocatalytic property of a novel dumbbell-shaped ZnO microcrystal photocatalyst, J. Hazard. Mater. 172 (2009) 1520–1526.
[6] N. Takahashi, K. Kaiya, K. Omichi, T. Nakamura, S. Okamoto, H. Yamamoto, Atmospheric pressure vapor-phase growth of ZnO using a chloride source, J. Cryst. Growth 209 (2000) 822–827.
[7] P. Mishra, R.S. Yadav, A.C. Pandey, Growth mechanism and photoluminescence property of flower-like ZnO nanostructures synthesized by starch-assisted sonochemical method, Ultrason. Sonochem. 17 (2010) 560–565.
[8] S. Suwanboon, structural and optical properties of nanocrystalline ZnO powder from sol–gel method, Sci. Asia 34 (2008) 31–34.
[9] X. Li, G. He, G. Xiao, H. Liu, M. Wang, Synthesis and morphology control of ZnO nanostructures in microemulsions, J. Colloid Interface Sci. 333 (2009) 465–473.
[10] K. Thongsuriwong, P. Amornpitoksuk, S. Suwanboon, The effect of aminoalcohols (MEA, DEA and TEA) on morphological control of nanocrystalline ZnO powders and its optical properties, J. Phys. Chem. Solids 71 (2010) 730–734.
[11] Z. Yang, L. Lv, Y. Dai, Z. Xv, D. Qian, Synthesis of ZnO–SnO_2 composite oxides by CTAB-assisted co-precipitation and photocatalytic properties, Appl. Surf. Sci. 256 (2010) 2898–2902.
[12] H. Wang, C. Xie, W. Zhang, S. Cai, Z. Yang, Y. Gui, Comparison of dye degradation efficiency using ZnO powders with various size scales, J. Hazard. Mater. 141 (2007) 645–652.
[13] S. Suwanboon, P. Amornpitoksuk, A. Haidoux, J.C. Tedenac, Structural and optical properties of undoped and aluminium doped zinc oxide nanoparticles via precipitation method at low temperature, J. Alloys Compd. 462 (2008) 335–339.
[14] M. Bicer, I. Sisman, Controlled synthesis of copper nano/microstructures using ascorbic acid in aqueous CTAB solution, Powder Technol. 198 (2010) 279–284.
[15] A. Degen, M. Kosec, Effect of pH and impurities on the surface charge of zinc oxide in aqueous solution, J. Eur. Ceram. Soc. 20 (2000) 667–673.
[16] H. Usui, The effect of surfactants on the morphology and optical properties of precipitated wurtzite ZnO, Mater. Lett. 63 (2009) 1459–1492.
[17] M.S. Mohajerani, A. Lak, A. Simchi, Effect of morphology on the solar photocatalytic behavior of ZnO nanostructures, J. Alloys Compd. 485 (2009) 616–620.
[18] M.N.R. Ashfold, R.P. Doherty, N.G. Ndifor-Angwafor, D. Jason Riley, Y. Sun, The kinetics of the hydrothermal growth of ZnO nanostructures, Thin Solid Films 515 (2007) 8679–8686.
[19] Y. Ishikawa, Y. Shimizu, T. Sasaki, N. Koshizaki, Preparation of zinc oxide nanorods using pulsed laser ablation in water media at high temperature, J. Colloid Interface Sci. 300 (2006) 612–615.
[20] S. Suwanboon, P. Amornpitoksuk, P. Bangrak, Synthesis, characterization and optical properties of $Zn_{1-x}Ti_xO$ nanoparticles prepared via a high-energy ball milling technique, Ceram. Int. 37 (2011) 333–340.
[21] Z. Hung, D. Yan, M. Yang, X. Liao, Y. Kang, G. Yin, Y. Yao, B. Hao, Preparation and characterization of the biomineralized zinc oxide particles in spider silk peptides, J. Colloid Interface Sci. 325 (2008) 356–362.
[22] X. Zhao, Z. Chen, Y. Luo, L. Wang, Giant enhanced infrared and orange emissions of ZnO nanoparticles induced by rich oxygen atmosphere, Solid State Commun. 147 (2008) 447–451.
[23] W.S. Chiu, P.S. Khiew, M. Cloke, D. Isa, T.K. Tan, S. Radiman, R. Abd-Shukor, M.A.Abd. Hamid, N.M. Huang, H.N. Lim, C.H. Chia, Photocatalytic study of two-dimensional ZnO nanopellets in the decomposition of methylene blue, Chem. Eng. J. 158 (2010) 345–352.
[24] Y. Wang, X. Li, N. Wang, X. Quan, Y. Chen, Controllable synthesis of ZnO nanoflowers and their morphology-dependent photocatalytic activities, Sep. Purif. Technol. 62 (2008) 727–732.
[25] A. Mills, S. Le Hunte, An overview of semiconductor photocatalysis, J. Photochem. Photobiol. A 108 (1997) 1–35.